Top Catal (2015) 58:910–918
DOI 10.1007/s11244-015-0459-9

ORIGINAL PAPER

Pd Loading and Structure of Flame-Made Pd/$YFeO_{3\pm\delta}$

Ye Lu[1] · Sylvain Keav[1] · Alexandra E. Maegli[1] · Anke Weidenkaff[1,3] · Davide Ferri[2]

Published online: 18 August 2015

Abstract The interactions between a platinum-group metal (PGM) and a perovskite-type oxide are complex since the latter can accommodate the former in its structure, simply act as a support or, in specific cases, reversibly switch between these two behaviours, depending on the redox environment. Despite promising performances as oxidation catalysts, Y-based perovskite-type oxides are far less studied than their La-based counterparts and their interactions with PGM need to be better understood. The morphology, coordination and oxidation state of Pd species in Pd-doped $YFeO_{3\pm\delta}$ catalysts prepared by flame spray synthesis were investigated in dependence on Pd loading in the range of 0–2.5 wt%. Their thermal stability was assessed by calcination of the flame-made materials at 700 °C. Fresh and calcined samples were thoroughly characterized by STEM, N_2-physisorption, XRD, XPS, DRIFTS and OSCC. Pd species were predominantly in the form of metallic nano-particles supported on $YFeO_{3\pm\delta}$. The size of these nano-particles increased with increasing loading as evidenced by DRIFTS. XPS facilitated the identification of Pd^{2+} species in strong interaction with the hexagonal $YFeO_3$ lattice, suggesting the partial incorporation of noble metal ions in the perovskite-type structure. After calcination at 700 °C, this contribution vanished in the catalysts containing at least 2 wt % Pd. The catalysts were tested for methane oxidation under stoichiometric conditions up to 850 °C. The catalyst with 2 wt% Pd exhibited the highest CH_4 oxidation activity. Reduction of the Pd content to 0.5 wt% resulted in the shift of the 50 % CH_4 conversion by only ca. 40 °C. Hence, flame-made Pd/$YFeO_{3\pm\delta}$ demonstrated to be a suitable material to maintain CH_4 conversion with reduced noble metal content.

Keywords Pd loading · Flame-spray synthesis · $YFeO_3$ · Methane oxidation

1 Introduction

Perovskite-type oxides are common oxidation catalysts [1, 2]. They are also used as catalyst supports for various applications where a metal active phase is required to improve the low temperature activity characteristics. The interaction between the perovskite-type oxide and platinum group metals (PGM) has generated considerable interest because of the possibility to produce more durable catalysts. The perovskite-type oxide is able to accommodate PGM ions within its structure and to segregate them in form of metal nano-particles when exposed to reducing environments [3]. This property is of great potential for automotive catalysis because in principle it allows to protect the precious metal active phase from sintering phenomena induced, for example, by exposure to high temperature. The property is of broader interest because it allows the design of materials with improved functionality.

PGM solubility in the perovskite structure has been reported for a variety of compositions [4]. Predictions based on theoretical simulations are also available [5]. In the case of Pd, only $LaFeO_3$ was shown to allow the

✉ Davide Ferri
davide.ferri@psi.ch

[1] Laboratory for Solid State Chemistry and Catalysis, Empa, Swiss Federal Laboratories for Materials Science and Technology, Ueberlandstrasse 129, 8600 Dübendorf, Switzerland

[2] Paul Scherrer Institut, 5232 Villigen, Switzerland

[3] Present Address: Institute for Materials Science, University of Stuttgart, Heisenbergstrasse 3, 70569 Stuttgart, Germany

occupation of the Fe sites over a broad concentration range [4]. $LaCoO_3$ is also a suitable host structure [6–8] but its reduction properties limit its use e.g. in automotive catalysis [9]. Although most attention has been given to lanthanum-based systems, yttrium-based ones can also present similar features. Recently, $YFeO_3$ was reported to show a similar behavior to $LaFeO_3$ with respect to the reversible segregation/incorporation in a perovskite-like structure [10]. $YFe_{0.95}Pd_{0.05}O_{3-\delta}$ demonstrated high CO oxidation activity after repeated reduction/oxidation at 450–500 °C, which is low temperature treatment compared to the one reported by the Daihatsu group for three-way catalysts (up to 800 °C) [11]. In $YFeO_3$, Pd stabilizes the hexagonal structure against the orthorhombic structure [10]. Pd is able to accommodate into the $YFeO_3$ structure, but Eyssler et al. [6] showed that the interaction between $YFeO_3$ and Pd (2 wt%) is temperature dependent. Calcination at 700 °C of the precursor salts created Pd ions, whereas calcination at 800 °C resulted in the development of Pd–O neighbours in the EXAFS spectra revealing formation of PdO-like particles. This latter material exhibited lower light-off temperature for lean methane oxidation in agreement with the observation that Pd particles on $LaFeO_3$ are more active than isolated ions within the $LaFe_{0.95}Pd_{0.05}O_{3-\delta}$ perovskite-type structure [12]. When prepared by flame-spray synthesis, $Pd/YFeO_3$ exhibits a very specific morphology, where Pd is predominantly in the form of segregated metal nano-particles on the perovskite-type oxide support. This makes it very active for CH_4 oxidation under stoichiometric conditions among various perovskite-type oxides [13]. In contrast to the behavior of $YFeO_3$ [10, 13], the CO oxidation activity of $BaCe_{1-x}Pd_xO_{3-\delta}$ is enhanced by integration of Pd in $BaCeO_3$ [14], which is attributed to the higher oxygen mobility obtained when Pd species in the form of Pd cations are accommodated in the perovskite structure.

Flame made 2 wt% $Pd/YFeO_3$ demonstrated the most active for CH_4 oxidation under stoichiometric conditions compared to catalysts based on other $ABO_{3\pm\delta}$ perovskite-type oxides (A = La, Y; B = Mn, Fe) and loaded with the same amount of Pd [13]. The present work focuses on a series of Pd-doped $YFeO_{3\pm\delta}$ catalysts prepared by flame spray synthesis (FSS) with increasing Pd content. We aim at characterizing the interactions between the PGM and the perovskite-type oxide at different Pd loadings and at determining how these interactions change between the fresh and the calcined materials. The methane oxidation activity of the samples is briefly discussed in relationship with their structure. We show that Pd particles increasingly deposit on $YFeO_3$ with increasing Pd content. The initial fraction of ionic Pd strongly interacting with $YFeO_3$ decreases in the same order.

2 Experimental

$YFeO_{3\pm\delta}$ and $Pd/YFeO_{3\pm\delta}$ perovskite-type oxides containing nominal 0.5, 1, 2 and 2.5 wt% Pd were prepared by FSS as described earlier [13]. Briefly, a 1:3 mixture of deionized water and *N*,*N*-dimethylformamide (DMF, 99 %, Sigma-Aldrich) was used as solvent of the metal nitrate precursors and sprayed in an acetylene–air flame. After synthesis, all samples were calcined at 700 °C for 2 h in air. Samples are hereafter labelled xPd/YFO, where x is the Pd weight content.

The specific surface area (SSA) and the reduction behaviour of the catalysts were measured using a QuantaChrom ChemBET 3000 instrument. Prior to the measurement, all samples were degassed in pure N_2 at 200 °C for 30 min. The SSA was determined using the single-point BET method in 30 vol% N_2/He. Temperature programmed reduction by hydrogen (H_2-TPR) was performed between 25 and 900 °C at 5 °C/min in 5 vol% H_2/He (20 ml/min).

The phase composition of fresh and aged catalysts was analysed by X-ray diffraction (X'Pert Pro PANalytical) using monochromatic Cu Kα1 radiation ($\lambda = 1.54$ Å). Phase identification was performed using the ICDD reference database in the *X'Pert Highscore Plus* software.

The morphology of the catalysts was observed using a Jeol 2200FS transmission electron microscope (TEM) equipped with a 200 kV field emission gun and a high-angle annular dark field detector for STEM mode (HAADF-STEM) providing images with atomic number ($Z^{1.5-1.8}$) contrast [15]. The local composition was determined by energy dispersive X-ray spectroscopy (EDS). The palladium particle size was measured using the software *ImageJ* by counting ca. 60 particles [16].

The oxygen storage capacity complete (OSCC, defined as the total amount of oxygen desorbed from the sample under reducing atmosphere) [17] of calcined catalysts was determined under static conditions in 5 vol% H_2/Ar at 400 °C (70 min) using the thermogravimetric method [18]. The observed weight loss was converted into the corresponding oxygen content assuming that the sample is fully oxidized in its initial state.

Diffuse reflectance infrared Fourier transform spectroscopy (DRIFTS) data were collected using a VERTEX 70 FT-IR spectrometer (Bruker) equipped with a reaction chamber (HVC-DRP-2, Harrick) and a liquid-nitrogen cooled MCT detector. Prior to CO adsorption, the samples were exposed to 20 vol% O_2/Ar (50 ml/min) at 500 °C for 30 min, followed by reduction at 300 °C for 30 min in 10 vol% H_2/Ar. CO adsorption was followed at room temperature in flowing 5 vol% CO/Ar.

X-ray photoelectron spectroscopy (XPS) measurements were performed on powders using monochromatic Al Kα

radiation and a hemispherical capacitor electron-energy analyser equipped with a channel plate and a position-sensitive detector (PHI Quantum 2000). The beam diameter was typically 100 μm. All the spectra were corrected for electrical charging by positioning the C1s peak of adventitious carbon at 284.8 eV.

The light-off profiles of the catalysts were obtained in a simulated exhaust mixture comprising 7000 ppm CO, 1300 ppm CH_4, 1600 ppm NO_x and 5300 ppm O_2 (He balance; 100 ml/min; GHSV = 60,000 h^{-1}). The reaction was performed between 25 and 850 °C in a quartz-tube reactor (d = 6 mm) using 100 mg of 150–200 μm catalyst particles diluted with the same volume and sieved fraction of sea sand and firmly fixed in the middle of the reactor between two quartz wool plugs. Prior to reaction, the catalysts were treated in 20 vol% O_2/He (50 ml/min) at 700 °C for 2 h. No further treatment was performed between consecutive activity runs. The outlet of the reactor was analysed with a gas chromatograph (Agilent 3000A Micro GC) equipped with PoraPLOT-Q and molecular sieve 5Å columns.

3 Results and Discussion

The structural properties of the catalysts are summarized in Table 1. The Pd contents measured by ICP-OES are close to the nominal ones. The SSA of fresh samples is in the range of 21–36 m^2/g. After calcination, all samples except 1Pd/YFO (10 m^2/g) exhibit similar SSA (17–19 m^2/g). There is no obvious correlation between Pd loading and SSA. All fresh catalysts exhibit similar XRD patterns (not shown) and predominantly contain hexagonal $YFeO_{3\pm\delta}$ with monoclinic Y_2O_3 as the secondary phase as observed earlier [13]. The overlap of the diffraction peaks of the two phases prevents from quantifying the fraction of Y_2O_3. Calcination at 700 °C has been shown to remove the unburnt precursors and to improve the phase purity of the flame-made materials [13]. However, no perceptible difference is observed between the XRD patterns before and after calcination. Traces of orthorhombic $YFeO_3$ (PDF: 01-086-0171) are clearly identified in YFO (Fig. 1), which progressively disappear with increasing Pd loading confirming that the hexagonal $YFeO_3$ is stabilized by the presence of Pd [10]. The low signal-to-noise ratio and the sharp reflections confirm the initial nano-size and the high

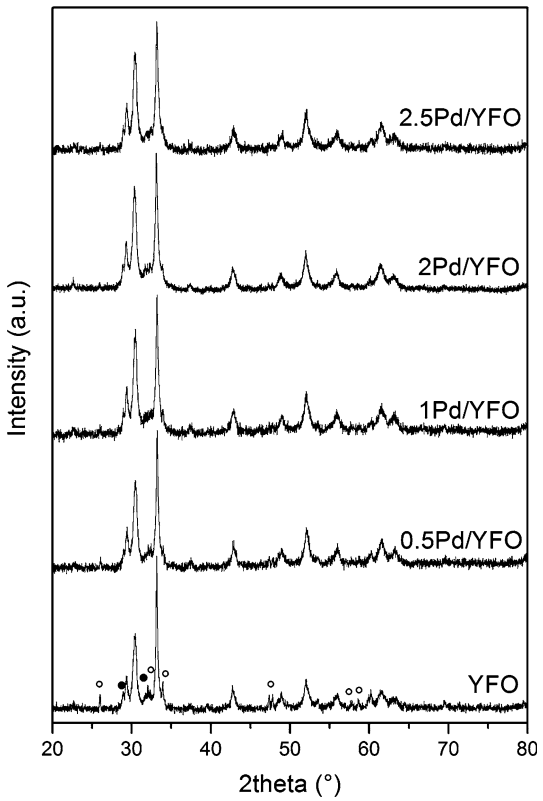

Fig. 1 XRD patterns of calcined xPd/YFO catalysts (*open circle* orthorhombic $YFeO_3$; *closed circle* Y_2O_3)

Table 1 BET surface area, Pd content, phase composition and OSCC of $Pd/YFeO_{3\pm\delta}$

Entry	Pd content[a]		SSA (m^2/g)		XRD[c]	OSCC[d]	Particle size[e] (nm)
	wt%	mol%	Fresh	Calc.[b]		μmol O_2/g	
YFO	0	0	27	19	h +Y_2O_3 + o	416	–
0.5Pd/YFO	0.46	0.00835	25	18	h + Y_2O_3	424	n.a.
1Pd/YFO	0.91	0.01655	21	10	h + Y_2O_3	466	n.a.
2Pd/YFO	1.75	0.03196	36	19	h + Y_2O_3	504	3.5 ± 1.4
2.5Pd/YFO	2.27	0.04156	33	17	h + Y_2O_3	563	5 ± 2

[a] Determined by ICP-OES

[b] 700 °C, 2 h in air

[c] *h* hexagonal; *o* orthorhombic; Y_2O_3 in the monoclinic structure

[d] Oxygen storage capacity complete at 400 °C (by TG analysis)

[e] Pd particle size measured from STEM images. *n.a.* not available

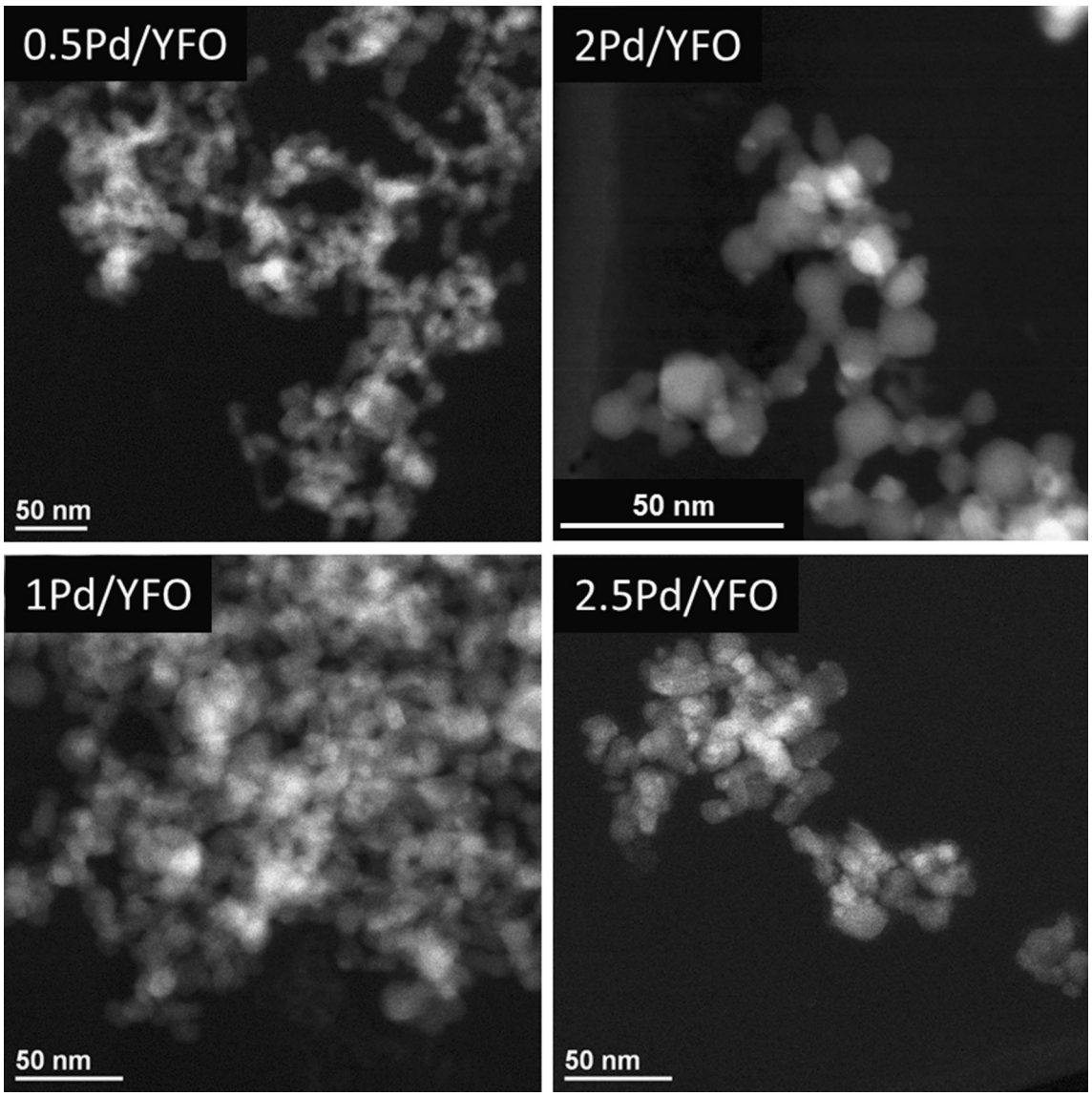

Fig. 2 HAADF-STEM of calcined xPd/YFO catalysts

crystallinity of the perovskite-type catalysts produced by FSS, respectively. No diffraction peaks related to Pd species are observed, suggesting that Pd is well dispersed in all catalysts. Also, the d spacing of the hexagonal phase does not change as a result of the presence of Pd since the peak position remained the same for all samples. Consequently, the microstructure of the calcined catalysts was investigated by HAADF-STEM (Fig. 2). Pd is found mainly in the form of PdO nano-particles dispersed on perovskite-type oxide particles of ca. 20 nm in diameter. In 2Pd/YFO [13] and 2.5Pd/YFO catalysts, it is readily seen from the image contrast that PdO particles are distributed on the support, with an average size of 3.5–5 nm (Table 1). Despite the clear identification of PdO particles, a possible fraction of atomically dispersed palladium, and possibly interacting with $YFeO_3$ cannot be excluded. On the other hand, the poor image contrast prevents from detecting particles in 0.5Pd/YFO and 1Pd/YFO. The phase composition was confirmed by EDS analysis.

The reduction characteristics of the calcined catalysts were studied by H_2-TPR (Fig. 3). The TPR profile of Pd-free $YFeO_3$ is characterized by the reduction of Fe^{n+} species above 300 °C in amorphous or secondary species not detected by XRD [12, 19, 20] and by the high temperature (650 °C) reduction of $YFeO_3$ to Y_2O_3 and Fe [21]. These Fe^{n+} species not included in the perovskite structure are consistent with the observation of Y_2O_3 by XRD. Addition of Pd changes the H_2-TPR profiles substantially.

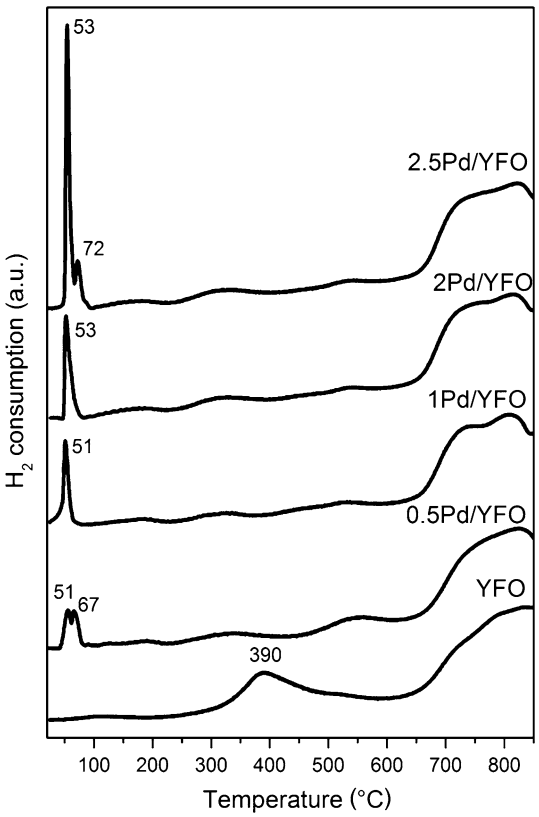

Fig. 3 H_2-TPR profiles of calcined xPd/YFO catalysts

A sharp reduction peak appears around 50 °C in the Pd/YFO series, which is readily assigned to the reduction of Pd^{2+} to Pd^0. The perovskite-type oxide can stabilize Pd against reduction up to ca. 300 °C as a result of the formation of a solid solution [12]. The low reduction temperature observed in the YFO-based samples suggests a relatively low interaction between Pd and $YFeO_3$. H_2 consumption increases with increasing Pd loading, which corroborates the formation of increasingly dispersed PdO particles.

Shallow H_2 consumption events at 200, 300 and 550 °C may evidence reduction of Fe^{n+} and Pd^{n+} species but their attribution is not straightforward.

The oxygen storage capacity complete (OSCC) values are given in Table 1. OSCC increases with increasing Pd content. Because of the similarity of SSA and the identical phase composition of the samples, this variation is attributed to the increasing amount of Pd. In comparison to the Pd-free material, the OSCC increase in samples containing 1, 2 and 2.5 wt% Pd is about 5 mmol(O_2)/g(Pd). This supports the assumption that in these samples most of Pd is not strongly interacting with $YFeO_3$ and is in the form of PdO particles, which are expected to release 4.7 mmol(O_2)/g(Pd). This observation is not verified in the low loaded sample. 0.5Pd/YFO releases only 1.7 mmol(O_2)/g(Pd) more than YFO. We can speculate that either the orthorhombic $YFeO_3$ secondary phase observed by XRD in YFO contributes to OSCC or that, at low noble metal content, most of Pd species do not contribute to the OSCC. The latter phenomenon could be the result of the strong interaction between Pd and $YFeO_3$ and the partial incorporation of Pd into the host lattice.

This issue was addressed using XPS. The photoelectron spectra of the Pd 3d core level of both fresh and calcined samples are shown in Fig. 4. In general, depending on the nature of Pd species, the binding energy (BE) of Pd $3d_{5/2}$ level varies between 335 and 335.4 eV for metallic Pd, 336.3–336.6 eV for $Pd^{II}O$ and 337.9–338.2 eV for $Pd^{IV}O_2$ [22–24]. The spectra of all fresh catalysts show a clear feature at 337.3 eV that is attributed to Pd^{n+} ($n > 2$) or Pd^{2+} ions in unusual coordination environment [25, 26]. Li et al. attributed the same signal to Pd^{2+} dissolved in the hexagonal host [10]. This species cannot be identified by XRD or HAADF-STEM. It could correspond to one or more of the minor reduction events observed in the H_2-TPR profiles. X-ray absorption spectroscopy is also ambiguous since Pd in the coordination environment expected from the structure of $YFeO_{3\pm\delta}$ [10] does not possess a defined signature in the near edge region [6]. The XANES spectra of the calcined samples (not shown) do not present significant difference compared to a typical supported PdO catalyst.

A second signal at lower BE (335.2 eV) in the photoelectron spectra of the fresh samples of Fig. 4 unequivocally confirms the presence of metallic Pd for higher loading than 1 wt%. This signal intensifies with increasing Pd loading indicating that Pd nano-particles increasingly deposit on the mixed oxide support that is in agreement with the STEM observation. For low loadings (≤1 wt%), this signal is slightly shifted to higher BE, indicating a possible contribution of Pd^{2+}. The XPS data of fresh 0.5Pd/YFO is comparable with that obtained for $YFe_{0.95}Pd_{0.05}O_{3\pm\delta}$ prepared by the citric acid route and providing Pd in intimate contact with the $YFeO_3$ lattice [6]. This may suggest that a similar Pd^{n+} species is obtained by the flame synthesis. The XPS data of the fresh catalysts suggest also that the solubility of Pd in $YFeO_3$ prepared by FSS is 0.5 wt% or lower since the XPS signature for Pd atoms organized into particles is already present. Metal nano-particles are progressively formed with increasing loading. Likely as a result of the flame conditions, e.g. higher temperature of the acetylene flame compared to a methane flame and higher energy density by the use of the DMF-based solvent, Pd atoms tend to agglomerate on the metal oxide surface rather than to combine with it. However, the trigonal bipyramid coordination that Pd atoms should adopt in the final mixed oxide [10] may also play a role in driving them to segregate rather than incorporate into $YFeO_3$. As a

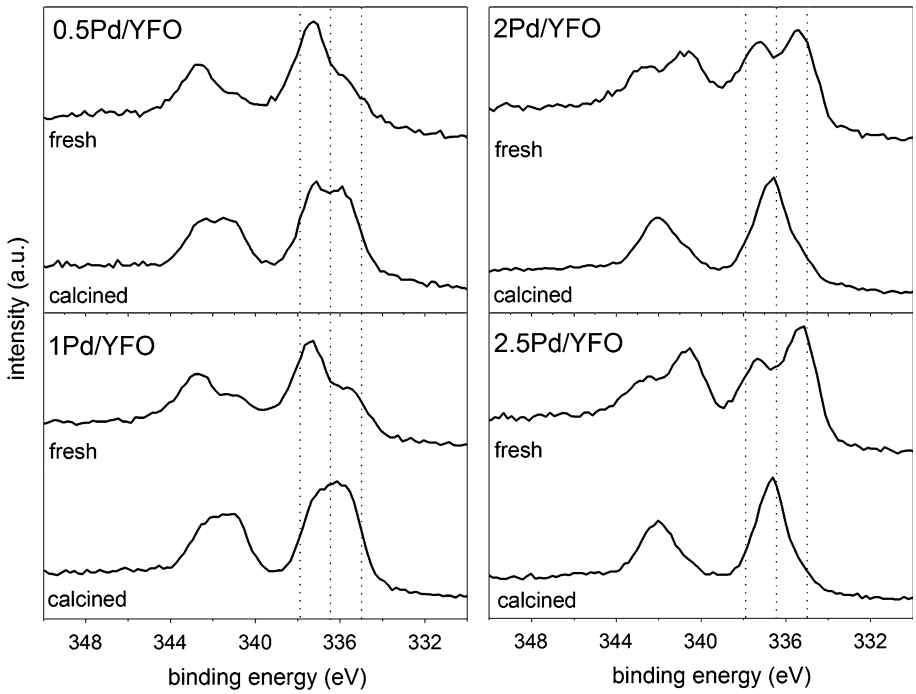

Fig. 4 X-ray photoelectron Pd 3d core level spectra of fresh and calcined xPd/YFO catalysts. *Vertical lines* indicate reference peak positions of Pd^0, Pd^{2+} and Pd^{4+} from the *right* to the *left*

consequence, similarly to what we suppose happens in the Pd–Y–Fe–O oxide obtained by the citric acid route [6], the Pd^{n+} species may reside close enough to the surface to be available to produce defined particles when the environmental conditions allow for it.

The effect of calcination at 700 °C on the XPS spectra is the production of a single photopeak at ca. 336.5 eV for high loading (>1 wt%), where only one species is present. The peak indicates that the Pd^{2+} species, thus PdO, have been stabilized after calcination as a result of oxidation of metallic Pd nano-particles. The full width at half maximum (FWHM) of the photopeak increases with decreasing Pd content. The signal is broad for low loading (≤1 wt%) and is evidently composed of two contributions clearly discernible for 0.5 wt%. The Pd^{2+} species coexists with Pd^{n+}. Therefore, the major effect of calcination is to oxidize Pd to PdO but Pd^{n+} may be present depending on loading. The presence of a considerable contribution from Pd^{n+} species in the XPS spectra of the low loaded samples accompanied by Pd^{2+} species supports the STEM results that do not present any tangible evidence of Pd nano-particles. In a similar manner to the FSS catalysts, calcination of $YFe_{0.95}Pd_{0.05}O_{3\pm\delta}$ prepared by the citric acid route at 800 °C destabilized the Pd ions interacting with $YFeO_3$ and caused a clear segregation of PdO, likely because of the low compatibility of Pd^{2+} and the $YFeO_3$ lattice. It should be observed that our considerations need to be limited only to that small portion of the material that is probed by XPS, thus preventing a definite assessment of the coordination of finely dispersed Pd species.

CO adsorption followed by DRIFTS (Fig. 5) provides supplementary structural information specifically associated with Pd that is not provided by electron microscopy. After reduction at 300 °C, CO adsorption at room temperature produces three major signals in the carbonyl region, i.e. at 2083 cm^{-1} (linearly adsorbed CO), 1982 cm^{-1} (μ_2-bridge bonded CO on Pd(100) faces and edges) and in the range of 1930–1750 cm^{-1} (broad band resulting from μ_3-hollow/multiple bonded CO on Pd(111) planes), which are assigned according to the available literature [27]. The spectrum of gas phase CO was taken from contact of CO with Pd-free YFO. The intensity variation among the catalysts that would correlate with the amount of available Pd is not obvious. Visibly, only the signal of bridge CO increases with increasing Pd content. The linearly adsorbed CO band is intense and symmetric in all catalysts suggesting a preferred adsorption on particle edges in well-defined adsorption geometry. This behaviour hints to the presence of well-dispersed Pd particles on $YFeO_3$. The major difference between the DRIFT spectra of the catalysts lies in the intensity ratio between the signal of linearly adsorbed CO and that of bridge-bonded CO (A_{2083}/A_{1982}). This ratio reflects the contribution of adsorption on Pd particle edges and corners relative to terrace sites [27]. The ratio increases in the order 2.5Pd/YFO (0.63) < 1Pd/YFO (0.90) < 2Pd/YFO (1.26) ~ 0.5Pd/YFO (1.29), where a high A_{2083}/A_{1982} ratio indicates a smaller average particle size of Pd. Hence, 2Pd/YFO and 0.5Pd/YFO exhibit the highest Pd dispersion among the xPd/YFO series.

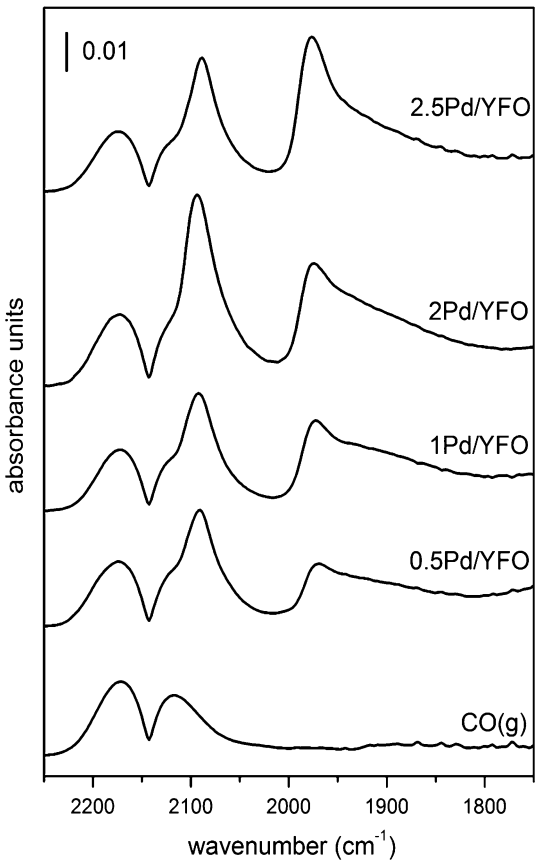

Fig. 5 DRIFT spectra of adsorbed CO on fresh xPd/YFO catalysts after reduction at 300 °C

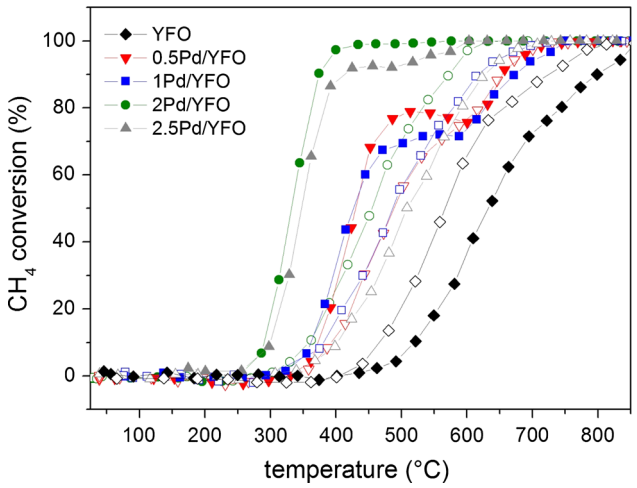

Fig. 6 CH_4 conversion profiles for the 1st (*open symbol*) and 3rd (*full symbol*) consecutive reaction runs on xPd/YFO catalysts

3.1 Catalytic Activity

The catalytic activity of the samples was evaluated between 25 and 850 °C in a feed comprising 7000 ppm CO, 1300 ppm CH_4, 1600 ppm NO and 5300 ppm O_2 ($\lambda = 1$) as shown in Fig. 6. 2Pd/YFO is the most active catalyst and displays the lowest $T_{50}^{CH_4}$, which is 116 °C lower than the value measured for the Pd-free material. The $T_{50}^{CH_4}$ decreases with increasing noble metal loading up to 2 wt% and then slightly increases. The low loading catalyst demonstrates comparable conversion profile to 1Pd/YFO. The lower Pd content causes a major deviation from the conversion profile of 1Pd/YFO for T > 550 °C. The larger the PdO particles segregated on $YFeO_3$, the lower the activity. Therefore 2.5Pd/YFO where Pd is present predominantly as PdO is the least active catalyst due to the lowest Pd dispersion. Activity of Pd-containing perovskite-type oxides for CH_4 oxidation is strongly influenced by the coordination state of Pd [12]. Exposed Pd at the surface of the support is crucial for activity, whereas Pd dissolved in the metal oxide lattice does not appear favourable. The XPS data demonstrate that the fraction of the segregated PdO increases with increasing loading and that mixed coordination states may be present depending on loading. Therefore, the effect of loading is further complicated because the fraction of exposed Pd organized in PdO particles deposited on $YFeO_3$ does not correspond to the total amount of available Pd.

All Pd/YFO catalysts experience the activation observed in our previous study [13]. For simplicity, only the light-off curves for CH_4 oxidation obtained during the 1st and 3rd cycles are shown in Fig. 6. The $T_{50}^{CH_4}$ values obtained in each reaction cycle are reported in Table 2. The CH_4 oxidation activity is largely improved in the 2nd reaction run (not shown) and preserved in the 3rd one. After the 3rd reaction cycle, 0.5Pd/YFO exhibits up to 10 % higher CH_4 conversion around 400–600 °C than 1Pd/YFO. However, a prominent kink in the methane conversion profile is observed between 500 and 650 °C for the two catalysts in the 3rd activity run. Similarly, 2.5Pd/YFO exhibits ca. 92 % conversion over a plateau extending from 400 to ca. 500 °C before a new increase to full conversion.

Based on the previous observations from the electron microscopy and XRD study of the used catalyst [13],

Table 2 $T_{50}^{CH_4}$ of xPd/YFO during each of consecutive three reaction runs

Entry	$T_{50}^{CH_4}$ (°C)		
	1st run	2nd run	3rd run
YFO	566	617	632
0.5Pd/YFO	486	422	430
1Pd/YFO	486	406	427
2Pd/YFO	450	333	332
2.5Pd/YFO	509	366	347

activation is induced by the formation of large metal Pd particles and by the concurrent sintering of $YFeO_3$. Therefore, the activity in the consecutive reaction runs involves different material properties compared to the calcined flame-made materials of the first activity run. In the absence of a detailed characterization of the used catalysts, we consider that all samples undergo similar Pd growth accompanied by $YFeO_3$ particle sintering. As demonstrated in a previous work [28], we also speculate that all Pd is now in the form of segregated metallic Pd particles, which are responsible for the catalytic activity during the second and third activity runs. Despite reduction and likely growth, these particles formed under reaction conditions remain prone to partial re-oxidation [28], which is essential for their redox activity. This is confirmed by the opposite trend of the activity of the Pd-free catalyst (Table 2) whose $T_{50}^{CH_4}$ increases after the first activity run as a result of the $YFeO_3$ particle growth. The presence of metal particles helps to clarify the drop of activity at intermediate temperatures for all samples but 2Pd/YFO. The partial metal state and the size of the particles decrease the fraction of active Pd atoms that should be involved in sustaining catalytic activity at low temperature. This effect is not visible in the conversion profile of 2Pd/YFO likely because this catalyst possesses a good combination of Pd content and available active surface atoms, which allows to limit the activity loss. 0.5Pd/YFO and 2Pd/YFO are the most promising catalysts in the series, which justifies the study of their ageing characteristics [28] and the transfer to cordierite substrates.

4 Conclusions

The effect of Pd loading on the structure and activity of flame-made $Pd/YFeO_3$ catalysts was investigated. Two major Pd species are observed after synthesis using XPS. The contribution of metallic Pd observed in the sample with 2 wt% Pd vanishes with decreasing loading in favour of Pd in stronger coordination environment with $YFeO_3$. After calcination, this latter species clearly persists up to 1 wt% Pd, while metallic Pd is converted into Pd^{2+}, likely in finely dispersed particles. The nature of the Pd species coordinated to $YFeO_3$ can be tentatively assessed only by XPS and by comparison with literature data. After calcination, catalysts with 0.5 and 2 wt% Pd show significant dispersion of Pd active species, which correlates with the highest CH_4 oxidation activity under stoichiometric conditions. Consecutive reaction cycles in the temperature range 25–850 °C produce a decrease of the temperature of 50 % CH_4 conversion that is Pd loading dependent. Beside 2 wt% $Pd/YFeO_3$, the most active among all catalysts, 0.5 wt% $Pd/YFeO_3$ exhibits comparable activity to 1 wt% $Pd/YFeO_3$. The exposure to high temperature during reaction likely causes a change in Pd speciation in favor of Pd nanoparticles with the consequent improvement of catalytic activity.

This work confirms that flame-made $YFeO_3$ is likely not a perfect host for Pd especially for high temperature reactions. However, some degree of interaction between Pd and $YFeO_3$ may be responsible for the performance of the low Pd content sample. Finally, the present data suggest that the solubility limit of Pd in the flame-made $YFeO_3$ is at 0.5 wt% Pd or below.

Acknowledgments The authors are grateful to the Swiss National Science Foundation (SNF) - National Research Program NFP62 'Smart Materials' (Project no. 406240-126127) and the COFUND program (EMPAPOSTDOCS Project no. PCOFUND-GA-2010-267161) for financial support. We are grateful to Dr. A. Pappacena (University of Udine, Italy) for support with OSCC measurements.

References

1. Pena MA, Fierro JLG (2001) Chem Rev 101:1981
2. Royer S, Duprez D (2011) ChemCatChem 3:24
3. Nishihata Y, Mizuki J, Akao T, Tanaka H, Uenishi M, Kimura M, Okamoto T, Hamada N (2002) Nature 418:164
4. Tanaka H, Taniguchi M, Uenishi M, Kajita N, Tan I, Nishihata Y, Mizuki J, Narita K, Kimura M, Kaneko K (2006) Angew Chem Int Ed 45:5998
5. Yanagisawa S, Uozumi A, Hamada I, Morikawa Y (2013) J Phys Chem C 117:1278
6. Eyssler A, Winkler A, Safonova O, Nachtegaal M, Matam SK, Hug P, Weidenkaff A, Ferri D (2012) Chem Mater 24:1864
7. Engelmann-Pirez M, Granger P, Leclerq G (2005) Catal Today 107–108:315
8. Chiarello GL, Grunwaldt JD, Ferri D, Krumeich F, Oliva C, Forni L, Baiker A (2007) J Catal 252:127
9. Tan I, Tanaka H, Uenishi M, Kaneko K, Mitachi S (2008) J Ceram Soc Jpn 113:71
10. Li J, Singh UG, Schladt TD, Stalick JK, Scott SL, Seshadri R (2008) Chem Mater 20:6567
11. Uenishi M, Taniguchi M, Tanaka H, Kimura M, Nishihata Y, Mizuki J, Kobayashi T (2005) Appl Catal B Environ 57:267
12. Eyssler A, Mandaliev P, Winkler A, Hug P, Safonova O, Figi R, Weidenkaff A, Ferri D (2010) J Phys Chem C 114:4584
13. Lu Y, Michalow KA, Matam SK, Winkler A, Maegli AE, Yoon S, Heel A, Weidenkaff A, Ferri D (2014) Appl Catal B Environ 144:631
14. Singh UG, Li J, Bennett JW, Rappe AM, Seshadri R, Scott SL (2007) J Catal 249:349
15. Pennycook SJ (1989) Ultramicroscopy 30:58
16. Rasband WS (1997–2012) ImageJ. U.S. National Institutes of Health, Bethesda
17. Lambrou PS, Efstathiou AM (2006) J Catal 240:182
18. Mamontov E, Brezny R, Koranne M, Egami T (2003) J Phys Chem B 107:13007
19. Ciambelli P, Cimino S, Lisi L, Faticanti M, Minelli G, Pettiti I, Porta P (2001) Appl Catal B Environ 33:193
20. Zhang R, Alamdari H, Kaliaguine S (2006) J Catal 242:241
21. Carreiro L, Qian YT, Kershaw R, Dwight K, Wold A (1985) Mater Res Bull 20:619

22. Moulder JF (1995) Handbook of x-ray photoelectron spectroscopy: a reference book of standard spectra for identification and interpretation of XPS data. Physical Electronics Division, Perkin Elmer Corporation, Boca Raton
23. Kim KS, Gossmann AF, Winograd N (1974) Anal Chem 46:197
24. Marmede AS, Leclercq G, Payen E, Granger P, Gengembre L, Grimblot J (2002) Surf Interface Anal 34:105
25. Thompson P, Cox DE, Hastings JB (1987) J Appl Crystallogr 20:79
26. MondragonRodriguez GC, Kelm K, Heiskens S, Grunert W, Saruhan B (2012) Catal Today 184:184
27. Lear T, Marshall R, Lopez-Sanchez JA, Jackson SD, Klapötke TM, Bäumer M, Rupprechter G, Freund HJ, Lennon D (2005) J Chem Phys 123:1
28. Lu Y, Keav S, Marchionni V, Chiarello GL, Pappacena A, Di Michiel M, Newton MA, Weidenkaff A, Ferri D (2014) Catal Sci Technol 4:2919